THE JOURNAL OF PHYSICAL CHEMISTRY LETTERS
A JOURNAL OF THE AMERICAN CHEMICAL SOCIETY

pubs.acs.org/JPCL

Letter

Low Barrier for Exciton Self-Trapping Enables High Photoluminescence Quantum Yield in $Cs_3Cu_2I_5$

Young-Kwang Jung, Sunghyun Kim, Yong Churl Kim, and Aron Walsh*

Cite This: *J. Phys. Chem. Lett.* 2021, 12, 8447–8452

Read Online

ACCESS | Metrics & More | Article Recommendations | Supporting Information

ABSTRACT: The metal halide $Cs_3Cu_2I_5$ displays anomalous optical properties: an optical absorption onset in the ultraviolet region (~330 nm) with highly efficient luminescence in the blue region (~445 nm). Although self-trapped exciton formation has been proposed as the origin of giant Stokes shift, its connection to the photoluminescence quantum yield exceeding 90% remains unknown. Here, we explore the photochemistry of $Cs_3Cu_2I_5$ from first-principles and reveal a low energy barrier for exciton self-trapping associated with Cu−Cu dimerization. Kinetic analysis shows that the quantum yield of blue emission in $Cs_3Cu_2I_5$ is sensitive to the excited carrier density due to the competition between exciton self-trapping and band-to-band radiative recombination.

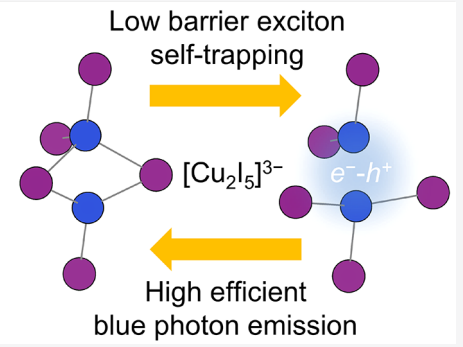

Metal halides with low-dimensional crystal structures have gained attention for applications in light emission due to their high photoluminescence quantum yield (PLQY).[1−5] The fact that these metal halides exhibit a high bulk PLQY, without preparing them in nanocrystal form, makes them an interesting class of optoelectronic materials. One characteristic feature is a large Stokes shift—the difference between absorbed and emitted photon energy—which is usually attributed to the formation of self-trapped excitons (STEs). STE indicates the state where a photoexcited electron−hole pair is stabilized and trapped at a lattice site. This phenomenon is the result of strong electron−phonon coupling and can be enhanced by a soft crystal host.[6] Via STE emission, $(C_6H_5CH_2NH_3)_3InBr_6$ shows a PLQY of >35%[7] in orange emission, $CsCu_2I_3$ shows a PLQY of >15%[8] in yellow emission, $(C_4N_2H_{14}Br)_4SnBr_6$ shows a PLQY of >90%[9] in green emission, and $Cs_3Cu_2I_5$ shows a PLQY of >90%[2] in blue emission in their single crystal phase.

Despite the high PLQY, light-emitting diodes (LEDs) made with these materials have not yet succeeded in reaching a high external quantum efficiency (EQE), with reported performance of <0.3%.[10−12] This could be due to not only a lack of device optimization but also a lack of our understanding of the emission processes happening within low-dimensional metal halides. Indeed, two outstanding questions are (i) why self-trapping occurs so efficiently and (ii) how self-trapped exciton emission competes against intrinsic band-to-band transitions. Answers are necessary to explain why this class of materials exhibit such a high PLQY and to offer a rational avenue of further enhancing performance.

We selected $Cs_3Cu_2I_5$ as the model system for a theoretical investigation since the compound is an established example of STE emission. The optical spectrum of the related $CsCu_2I_3$ system has previously been calculated by using the two-particle GW+BSE approach,[13] which found an average exciton binding energy of 80 meV in the absence of structural relaxation. By considering a distorted primitive unit cell, Lian et al.[14] estimated a binding energy of 580 meV in $Cs_3Cu_2I_5$; however, the pathway was not investigated. Here, the energy landscape and kinetics were probed on the basis of first-principles hybrid density functional theory (DFT) calculations. We first assess the optical properties of the material, i.e., a high-frequency dielectric function and an absorption coefficient, that originate from its intrinsic bulk electronic structure. Then we move on to explicit modeling of exciton formation including the STE emission energy and self-trapping barrier. On the basis of these quantities, we evaluate the rates of band-to-band recombination and STE emission, and consequently, we predict the quantum yield of blue emission as a function of the excited carrier concentration.

Pristine Crystal. Because we have recently provided analysis of crystal structure and electronic band structure of $Cs_3Cu_2I_5$,[15] here we briefly summarize them. In Figure 1a, the primitive unit cell (space group *Pnma*) of $Cs_3Cu_2I_5$ that contains 40 atoms is shown. The calculated lattice constants of a_0 = 10.06 Å, b_0 = 11.53 Å, and c_0 = 14.15 Å are in good agreement with

Received: July 13, 2021
Accepted: July 27, 2021
Published: August 26, 2021

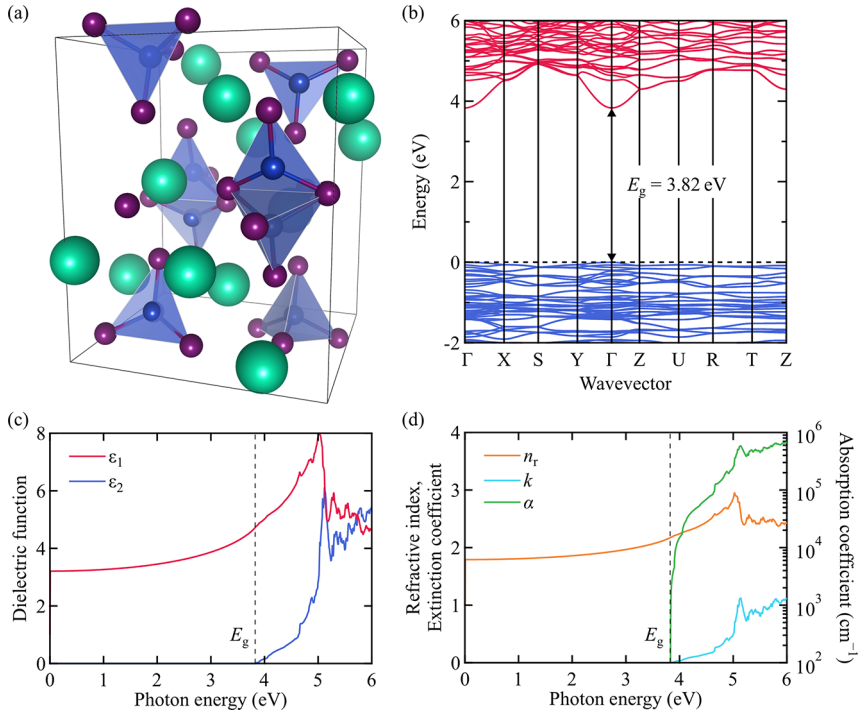

Figure 1. (a) Crystal structure of $Cs_3Cu_2I_5$, where Cs, Cu, and I atoms are represented as green, blue, and purple balls. (b) Electronic band structure. (c) Real (ε_1) and imaginary (ε_2) parts of the optical dielectric function. (d) Refractive index (n_r), extinction coefficient (k), and absorption coefficient (α). The vertical dashed lines in (c) and (d) indicate the calculated fundamental band gap of the material.

X-ray diffraction analysis (a_0^{exp} = 10.19 Å, b_0^{exp} = 11.66 Å, and c_0^{exp} = 14.40).[2] The calculated direct band gap within the nonlocal HSE06[16,17] level of theory is 3.82 eV at the Γ point, which shows excellent agreement with the experimentally determined band gap of 3.8 eV.[10]

On the basis of the DFT/HSE06 wave functions, we obtained maximally localized Wannier functions with the disentanglement scheme proposed by Souza et al.,[18] from which we calculated the frequency-dependent dielectric function. Despite the absence of connectivity between $[Cu_2I_5]^{3-}$ anion clusters, the band structure shows a dispersive lower conduction band, while the higher valence band is found to be flat (see Figure 1b). It is a special behavior of Cu-based low-dimensional metal halides when compared with other Pb- or Sn-based low-dimensional metal halides whose conduction band edge and valence band edge are both flat in reciprocal space.[19,20]

The complex dielectric function of $Cs_3Cu_2I_5$, calculated within independent particle approximation, is plotted in Figure 1d. The real part (ε_1) at photon energy → 0 eV is the optical dielectric constant (ε_∞). We obtained ε_∞ = 3.2 from the Wannier interpolation with HSE06, which is slightly lower than ε_∞ = 3.8 calculated from density-functional perturbation theory (DFPT) using the PBEsol[21] exchange-correlation functional.[15] This originates from the band gap underestimation by DFT/PBEsol as the optical dielectric constant is inversely proportional to the band gap.[22] From the dielectric function, the refractive index (n_r) and extinction coefficient (k) can be determined from

$$n_r = \sqrt{\frac{\sqrt{\varepsilon_2^1 + \varepsilon_2^2} + \varepsilon_1}{2}}, \qquad k = \sqrt{\frac{\sqrt{\varepsilon_2^1 + \varepsilon_2^2} - \varepsilon_1}{2}} \tag{1}$$

which are the solutions of the $\varepsilon_1 + i\varepsilon_2 = (n_r + ik)^2$ relationship. Furthermore, the optical absorption coefficient (α) can be calculated following

$$\alpha = \frac{4\pi k}{\lambda} \tag{2}$$

where λ is the wavelength of photon. As shown in Figure 1d, $Cs_3Cu_2I_5$ has a n_r of 1.8−1.9 in the visible light range, and it reaches 3 in the ultraviolet (UV) region. A stiff onset of absorption is also observed at the calculated band gap 3.82 eV, and α rapidly reaches ∼10^5 cm^{-1}. Although the calculated optical spectra of the perfect $Cs_3Cu_2I_5$ crystal can explain the onset of absorbance in the UV region, it cannot explain sub-band-gap emission, which implies the blue photon emission in the material is not a bulk response.

Self-Trapped Excitons. The sub-band-gap emission mediated by STE has been suspected as the origin of the large Stokes shift in $Cs_3Cu_2I_5$[2,10] and other low-dimensional metal halide compounds such as K_2CuCl_3,[23] Cs_4SnBr_6,[24] and $MA_4Cu_2Br_6$.[25] There have been attempts to simulate STE assisted emission energies in these materials,[26−28] but the shape of potential energy surface for STE emission process remains unknown. We construct the configurational coordinate diagram associated with the ground-state singlet (S_0), excited-state singlet (S_1), and excited-state triplet (T_1) configurations in $Cs_3Cu_2I_5$ based on the Δ self-consistent field (ΔSCF) method combined with the HSE06 functional (see Figure 2a). Because STE is associated with a highly localized state and local lattice distortion, including structural relaxation of the excited state in a supercell is critical. Although many-body perturbation theory (e.g., GW+BSE[29]) can accurately describe electron−hole interactions, the atomic forces and total energy of crystals are poorly defined. Hence, we adopted the ΔSCF method as it

https://doi.org/10.1021/acs.jpclett.1c02252
J. Phys. Chem. Lett. 2021, 12, 8447−8452

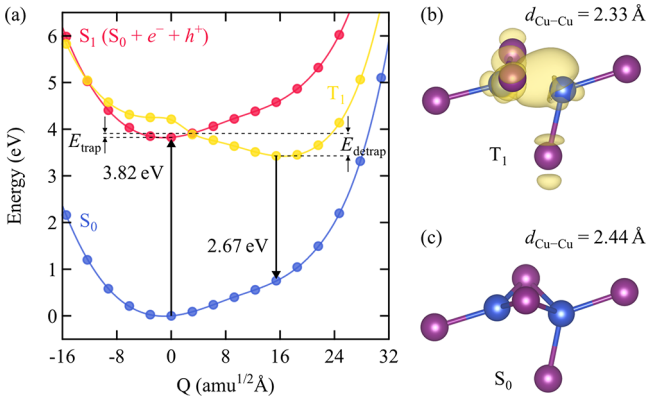

Figure 2. (a) Configuration coordinate diagram of ground singlet (S_0), excited singlet (S_1), and triplet (T_1) state within $Cs_3Cu_2I_5$. Associated absorption and emission energies are indicated by the black arrows. The black dashed lines display the exciton self-trapping barrier (E_{trap}) and detrapping barrier (E_{detrap}). Atomic structure of the $[Cu_2I_5]^{3-}$ anion cluster in the (b) T_1 state and (c) S_0 state. d_{Cu-Cu} represents the distance between two Cu atoms in the cluster. The triplet spin density is illustrated as yellow clouds in (b).

has shown agreement with measurements for copper based low-dimensional metal halides.[27,28]

When $Cs_3Cu_2I_5$ absorbs light that has a energy exceeding the band gap (3.82 eV), a vertical transition from S_0 to from S_1 can occur. The charge carriers (i.e., e^- and h^+) generated by light could recombine radiatively (S_1 to S_0 vertical transition), emitting photons with the band gap energy, or could form STEs via coupling with phonons (S_1 to T_1 horizontal transition). Thus, the energy barrier of the S_1 to T_1 transition is a key factor that governs kinetics of the exciton self-trapping and consequently the quantum yield for STE emission. The exciton self-trapping barrier (E_{trap}) is 0.09 eV, whereas the exciton detrapping barrier (E_{detrap}) is calculated to be 0.48 eV. The large difference between E_{trap} and E_{detrap} indicates that most of generated STEs result in photon emission through the T_1 to S_0 vertical transition rather than dissociation of the triplet STEs to free carriers (T_1 to S_1 horizontal transition). The emission energy from T_1 to S_0 vertical transition is found to be 2.67 eV, which is in a good agreement with previous theoretical and experimental studies.[2,10,27,30] Moreover, no nonradiative decay path (T_1 to S_0 horizontal transition) was found in our calculation, which indicates blue photon emission is the primary process for STEs in $Cs_3Cu_2I_5$ to decay back to the ground state.

The local geometry of a $[Cu_2I_5]^{3-}$ anion cluster in its STE (T_1) state and ground (S_0) state is shown in Figure 2b,c. In the ground state, two I atoms reside in between two Cu atoms where they are forming bonds with both Cu atoms. Therefore, the anion cluster is formed of two combined CuI_3 trigonal-planar motif and CuI_4 tetrahedral motif. When a triplet exciton traps at $[Cu_2I_5]^{3-}$, it strengthens a Cu−Cu bond ~5% and breaks the cluster into two separate CuI_3 trigonal-pyramidal and CuI_2 angular motifs. Formation of a Cu−Cu dimer and deformation of Cu−X (X = Cl, Br, I) bonds are also observed in other Cu-based low-dimensional metal halides.[23,28]

First-Principles Quantum Yield. The final piece necessary to explain the high PLQY in $Cs_3Cu_2I_5$ is the kinetic balance between self-trapped exciton emission and intrinsic band-to-band recombination. As there is no crossing between T_1 and S_0 in configuration coordinate space, and E_{detrap} is much larger than E_{trap}, we assume that exciton self-trapping leads to phosphorescence. Then, we can calculate the quantum yield of STE emission (ϕ_{ste}) from

$$\phi_{ste} = \frac{k_{trap}n}{k_{trap}n + k_{rad}n^2} \tag{3}$$

where n is the excited carrier concentration, k_{trap} is the exciton self-trapping rate constant, and k_{rad} is the radiative (bimolecular) recombination rate constant. k_{trap} was estimated from the Eyring equation

$$k_{trap} = \frac{\kappa k_B T}{h} \exp\left(-\frac{E_{trap}}{k_B T}\right) \tag{4}$$

where κ is the transmission coefficient (here assumed to be 1) and h is the Planck constant. This yields a prefactor of 6.25×10^{12} s^{-1} at T = 300 K that is typical for exciton trapping.[31] A more rigorous description of this intersystem crossing would require matrix elements involving spin−orbit coupling,[32] which are not yet implemented for solid-state crystal calculations. On the other side, the radiative recombination rate constant (k_{rad}) was calculated as follows:

$$k_{rad} = \frac{1}{n_i^2}\frac{2\pi}{h^3c^2}\int_0^\infty n_r(E)^2\alpha(E)\exp\left(-\frac{E}{k_B T}\right)E^2\,dE \tag{5}$$

where n_i is the intrinsic carrier concentration, c is the speed of light, n_r is the refractive index, and α is the absorption coefficient.

The calculated k_{trap} and k_{rad} at 300 K are 2.18×10^{11} s^{-1} and 3.13×10^{-11} cm^3 s^{-1}, respectively. Adopting those values, we plotted change in reaction rate and quantum yield as a function of excited carrier concentration (n) at 300 K (see Figure 3). In

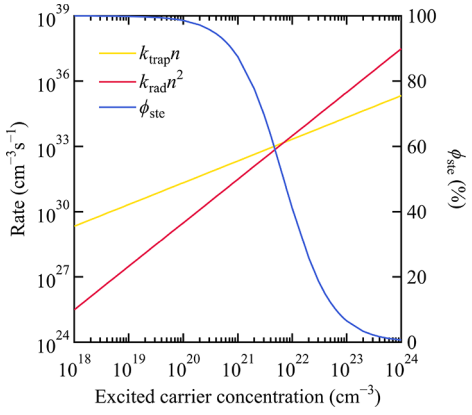

Figure 3. Excited carrier concentration-dependent exciton self-trapping rate ($k_{trap}n$), radiative recombination rate ($k_{rad}n^2$), and quantum yield of STE emission (ϕ_{ste}) at 300 K.

low n region ($n < 10^{20}$ cm^{-3}) ϕ_{ste} is predicted to be ~100%, which indicates most excited carriers undergo exciton self-trapping before they recombine through the band-to-band transitions. Indeed, an almost linear luminescence intensity vs excitation power (until 80 μJ cm^{-2} with a 315 nm laser source) relation during photoexcitation experiment was observed by Chen et al.[10] Their excitation power of 80 μJ cm^{-2} corresponds to a n of 1.27×10^{19} cm^{-3} for a 100 nm sample when an absorbance of 1 is assumed. On the other hand, in a higher n region ($n > 10^{22}$ cm^{-3}), ϕ_{ste} drops toward 0%, which means the

https://doi.org/10.1021/acs.jpclett.1c02252
J. Phys. Chem. Lett. 2021, 12, 8447−8452

majority of excited carriers recombine via S_1-to-S_0 transitions. Therefore, $Cs_3Cu_2I_5$ is an efficient blue emitter under photoexcitation for low n, but it will become a UV emitter under high current density. This analysis provides one factor for why high PLQY in low-dimensional metal halides cannot guarantee high EQE in LEDs.[10−12] We further note that this first model ignores both trap-mediated and Auger recombination mechanisms. Auger recombination, which is proportional to n^3, will result in a faster drop in ϕ_{ste} in a high excited carrier concentration region. The choice of an optimal excitation regime, depending on materials properties, will be key to maximize quantum yield of luminescence.

In conclusion, we have identified the self-trapping exciton structure of $Cs_3Cu_2I_5$ and developed a theoretical model to explain its optical properties. This material has a stiff onset of absorption and high absorption coefficient of $>10^5$ cm^{-1}. Self-trapped excitons can be efficiently generated due to the small self-trapping barrier of 0.09 eV. Moreover, we predict the quantum yield of STE emission for the crystal based on first-principles quantities. $Cs_3Cu_2I_5$ is found to have the quantum yield of STE emission that reaches 100% in the low carrier concentration region ($n < 10^{20}$ cm^{-3}), which explains the exceptional PLQY of >90% for blue emission. In the high excitation density regime ($n > 10^{22}$ cm^{-3}), however, the band-to-band radiative recombination process that results in UV emission becomes more dominant, and the quantum yield of STE emission decreases to 0%. Our model will support advanced computational simulations of light emission in crystals and support the accelerated discovery of optoelectronic materials. Further developments of the model, to include a wider range of recombination processes and more sophisticated electron−phonon interactions, are required for a complete description of carrier dynamics and lifetimes.

COMPUTATIONAL METHODS

Beyond the ground-state electronic band structure, our analysis of self-trapped excitation formation requires a description of optical transitions, as well as the potential energy landscape associated with the charge localization.

The underlying Kohn−Sham density functional theory (DFT)[33] calculations were performed via the Vienna Ab Initio Simulation Package (VASP)[34,35] where periodic boundary conditions are considered. Projector augmented-wave (PAW)[36,37] pseudopotentials were used where the valence states of Cs, Cu, and I are treated explicitly by 9 ($5s^25p^66s^1$), 17 ($2p^63d^{10}4s^1$), and 7 ($5s^25p^5$) electrons, respectively. We adopted the primitive unit cell and electronic wave functions of $Cs_3Cu_2I_5$ from our previous report.[15]

The optical dielectric function (ε) is derived from the optical conductivity (σ) following

$$\varepsilon = \frac{4\pi i}{\omega}\sigma \tag{6}$$

where σ of $Cs_3Cu_2I_5$ was calculated from the Kubo−Greenwood formula implemented in Wannier90[18,38,39] and ω is the angular frequency. With the HSE06 wave functions as the input, we set a high dense **k**-point sampling of 80 × 80 × 60 during the Wannier90 routine to obtain the stiff onset of absorption coefficient at the band gap of the material, which is unapproachable from a regular self-consistent DFT calculation. A comparison between optical spectra calculated internally in VASP with coarse **k**-point grid points of 3 × 3 × 2 and via Wannier90 with dense **k**-point grid points of 80 × 80 × 60 can be found in Figure S1.

To describe self-trapped exciton formation, a $\sqrt{2} \times \sqrt{2} \times 1$ supercell (80 atoms) of $Cs_3Cu_2I_5$ was employed. The ground state and excited state geometries were first optimized by using the PBEsol functional where a Γ-centered **k**-mesh of 2 × 2 × 2 and a plane-wave kinetic energy cutoff of 700 eV were set. To simulate the localized T_1 state, we manually gave a distortion to a single $[Cu_2I_5]^{3-}$ cluster in the supercell and performed a geometry optimization to find a symmetry-broken stationary point corresponding to the self-trapped configuration. The difference in atomic positions in the ground state S_0 and excited state T_1 geometries defines the configuration coordinate system. We then calculated the potential energy surface along this effective one-dimensional coordinate. For more quantitative results, we performed self-consistent HSE06 calculations for each point on the configurational coordinate path. To reduce the computational cost, we set the plane-wave kinetic cutoff energy to 400 eV. The CarrierCapture.jl[40] package was used for interpolation and identifying the crossing points between potential energy surfaces. The potential energy surface of S_1 was drawn by vertically shifting the S_0 curve by the band gap of $Cs_3Cu_2I_5$ calculated from HSE06, i.e., 3.82 eV. We note that the spin density for T_1 is well-confined at a single $[Cu_2I_5]^{3-}$ cluster within the given supercell size, while the spin density for the ground state configuration becomes delocalized (see Figure S2).

ASSOCIATED CONTENT

Supporting Information

The Supporting Information is available free of charge at https://pubs.acs.org/doi/10.1021/acs.jpclett.1c02252.

Comparison of the optical dielectric function calculated from Wannier90 with a dense **k**-point grid and VASP with a coarse grid; comparison of delocalized spin density and localized spin density in undistorted and distorted supercells; data access (PDF)

AUTHOR INFORMATION

Corresponding Author

Aron Walsh − *Department of Materials Science and Engineering, Yonsei University, Seoul 03722, Korea; Department of Materials, Imperial College London, London SW7 2AZ, U.K.;* orcid.org/0000-0001-5460-7033; Email: a.walsh@imperial.ac.uk

Authors

Young-Kwang Jung − *Department of Materials Science and Engineering, Yonsei University, Seoul 03722, Korea;* orcid.org/0000-0003-3848-8163

Sunghyun Kim − *Department of Materials Science and Engineering, Yonsei University, Seoul 03722, Korea; Department of Materials, Imperial College London, London SW7 2AZ, U.K.;* orcid.org/0000-0001-5072-6801

Yong Churl Kim − *Samsung Electronics Materials Research Complex, Samsung Advanced Institute of Technology (SAIT), Suwon 443-803, Korea*

Complete contact information is available at: https://pubs.acs.org/10.1021/acs.jpclett.1c02252

Notes

The authors declare no competing financial interest.

https://doi.org/10.1021/acs.jpclett.1c02252
J. Phys. Chem. Lett. 2021, 12, 8447−8452

■ ACKNOWLEDGMENTS

This research was supported by Creative Materials Discovery Program through the National Research Foundation of Korea (NRF) funded by Ministry of Science and ICT (2018M3D1A1058536). Computational resources have been provided by the KISTI Supercomputing Center (KSC-2018-CRE-0108). We are grateful to the UK Materials and Molecular Modelling Hub for computational resources, which is partially funded by EPSRC (EP/P020194/1).

■ REFERENCES

(1) Saidaminov, M. I.; Almutlaq, J.; Sarmah, S.; Dursun, I.; Zhumekenov, A. A.; Begum, R.; Pan, J.; Cho, N.; Mohammed, O. F.; Bakr, O. M. Pure Cs_4PbBr_6: Highly Luminescent Zero-Dimensional Perovskite Solids. *ACS Energy Lett.* **2016**, *1*, 840−845.

(2) Jun, T.; Sim, K.; Iimura, S.; Sasase, M.; Kamioka, H.; Kim, J.; Hosono, H. Lead-Free Highly Efficient Blue-Emitting $Cs_3Cu_2I_5$ with 0D Electronic Structure. *Adv. Mater.* **2018**, *30*, 1804547.

(3) Morad, V.; Shynkarenko, Y.; Yakunin, S.; Brumberg, A.; Schaller, R. D.; Kovalenko, M. V. Disphenoidal Zero-Dimensional Lead, Tin, and Germanium Halides: Highly Emissive Singlet and Triplet Self-Trapped Excitons and X-ray Scintillation. *J. Am. Chem. Soc.* **2019**, *141*, 9764−9768.

(4) Li, X.; Gao, X.; Zhang, X.; Shen, X.; Lu, M.; Wu, J.; Shi, Z.; Colvin, V. L.; Hu, J.; Bai, X.; et al. Lead-Free Halide Perovskites for Light Emission: Recent Advances and Perspectives. *Adv. Sci.* **2021**, *8*, 2003334.

(5) Li, M.; Xia, Z. Recent Progress of Zero-Dimensional Luminescent Metal Halides. *Chem. Soc. Rev.* **2021**, *50*, 2626−2662.

(6) Li, S.; Luo, J.; Liu, J.; Tang, J. Self-Trapped Excitons in All-Inorganic Halide Perovskites: Fundamentals, Status, and Potential Applications. *J. Phys. Chem. Lett.* **2019**, *10*, 1999−2007.

(7) Chen, D.; Hao, S.; Zhou, G.; Deng, C.; Liu, Q.; Ma, S.; Wolverton, C.; Zhao, J.; Xia, Z. Lead-Free Broadband Orange-Emitting Zero-Dimensional Hybrid $(PMA)_3InBr_6$ with Direct Band Gap. *Inorg. Chem.* **2019**, *58*, 15602−15609.

(8) Lin, R.; Guo, Q.; Zhu, Q.; Zhu, Y.; Zheng, W.; Huang, F. All-Inorganic $CsCu_2I_3$ Single Crystal with High-PLQY (≈ 15.7%) Intrinsic White-Light Emission via Strongly Localized 1D Excitonic Recombination. *Adv. Mater.* **2019**, *31*, 1905079.

(9) Zhou, C.; Lin, H.; Tian, Y.; Yuan, Z.; Clark, R.; Chen, B.; van de Burgt, L. J.; Wang, J. C.; Zhou, Y.; Hanson, K.; et al. Luminescent Zero-Dimensional Organic Metal Halide Hybrids with Near-Unity Quantum Efficiency. *Chem. Sci.* **2018**, *9*, 586−593.

(10) Chen, H.; Pina, J. M.; Yuan, F.; Johnston, A.; Ma, D.; Chen, B.; Li, Z.; Dumont, A.; Li, X.; Liu, Y.; et al. Multiple Self-Trapped Emissions in the Lead-Free Halide $Cs_3Cu_2I_5$. *J. Phys. Chem. Lett.* **2020**, *11*, 4326−4330.

(11) Liu, X.; Yu, Y.; Yuan, F.; Zhao, C.; Dong, H.; Jiao, B.; Wu, Z. Vacuum Dual-Source Thermal-Deposited Lead-Free $Cs_3Cu_2I_5$ Films with High Photoluminescence Quantum Yield for Deep-Blue Light-Emitting Diodes. *ACS Appl. Mater. Interfaces* **2020**, *12*, 52967−52975.

(12) Ma, Z.; Shi, Z.; Yang, D.; Li, Y.; Zhang, F.; Wang, L.; Chen, X.; Wu, D.; Tian, Y.; Zhang, Y.; et al. High Color-Rendering Index and Stable White Light-Emitting Diodes by Assembling Two Broadband Emissive Self-Trapped Excitons. *Adv. Mater.* **2021**, *33*, 2001367.

(13) Sun, J.; Ullrich, C. A. Optical properties of $CsCu_2X_3$ (X = Cl, Br, andI): A Comparative Study Between Hybrid Time-Dependent Density-Functional Theory and the Bethe-Salpeter Equation. *Phys. Rev. Mater.* **2020**, *4*, 095402.

(14) Lian, L.; Zheng, M.; Zhang, P.; Zheng, Z.; Du, K.; Lei, W.; Gao, J.; Niu, G.; Zhang, D.; Zhai, T.; et al. Photophysics in $Cs_3Cu_2X_5$ (X = Cl, Br, or I): Highly Luminescent Self-Trapped Excitons from Local Structure Symmetrization. *Chem. Mater.* **2020**, *32*, 3462−3468.

(15) Jung, Y.-K.; Han, I. T.; Kim, Y. C.; Walsh, A. Prediction of High Thermoelectric Performance in the Low-Dimensional Metal Halide $Cs_3Cu_2I_5$. *npj Comput. Mater.* **2021**, *7*, 51.

(16) Heyd, J.; Scuseria, G. E.; Ernzerhof, M. Hybrid Functionals Based on a Screened Coulomb Potential. *J. Chem. Phys.* **2003**, *118*, 8207−8215.

(17) Krukau, A. V.; Vydrov, O. A.; Izmaylov, A. F.; Scuseria, G. E. Influence of the Exchange Screening Parameter on the Performance of Screened Hybrid Functionals. *J. Chem. Phys.* **2006**, *125*, 224106.

(18) Souza, I.; Marzari, N.; Vanderbilt, D. Maximally Localized Wannier Functions for Entangled Energy Bands. *Phys. Rev. B: Condens. Matter Mater. Phys.* **2001**, *65*, 1−13.

(19) Jung, Y.-K.; Calbo, J.; Park, J.-S.; Whalley, L. D.; Kim, S.; Walsh, A. Intrinsic Doping Limit and Defect-Assisted Luminescence in Cs_4PbBr_6. *J. Mater. Chem. A* **2019**, *7*, 20254−20261.

(20) Chiara, R.; Ciftci, Y. O.; Queloz, V. I.; Nazeeruddin, M. K.; Grancini, G.; Malavasi, L. Green-Emitting Lead-Free Cs4SnBr6 Zero-Dimensional Perovskite Nanocrystals with Improved Air Stability. *J. Phys. Chem. Lett.* **2020**, *11*, 618−623.

(21) Perdew, J. P.; Ruzsinszky, A.; Csonka, G. I.; Vydrov, O. A.; Scuseria, G. E.; Constantin, L. A.; Zhou, X.; Burke, K. Restoring the Density-Gradient Expansion for Exchange in Solids and Surfaces. *Phys. Rev. Lett.* **2008**, *100*, 136406.

(22) Penn, D. R. Wave-Number-Dependent Dielectric Function of Semiconductors. *Phys. Rev.* **1962**, *128*, 2093.

(23) Creason, T. D.; McWhorter, T. M.; Bell, Z.; Du, M.-H.; Saparov, B. K_2CuX_3 (X = Cl, Br): All-Inorganic Lead-Free Blue Emitters with Near-Unity Photoluminescence Quantum Yield. *Chem. Mater.* **2020**, *32*, 6197−6205.

(24) Benin, B. M.; Dirin, D. N.; Morad, V.; Wörle, M.; Yakunin, S.; Rainò, G.; Nazarenko, O.; Fischer, M.; Infante, I.; Kovalenko, M. V. Highly Emissive Self-Trapped Excitons in Fully Inorganic Zero-Dimensional Tin Halides. *Angew. Chem.* **2018**, *130*, 11499−11503.

(25) Peng, H.; Yao, S.; Guo, Y.; Zhi, R.; Wang, X.; Ge, F.; Tian, Y.; Wang, J.; Zou, B. Highly Efficient Self-Trapped Exciton Emission of a $(MA)_4Cu_2Br_6$ Single Crystal. *J. Phys. Chem. Lett.* **2020**, *11*, 4703−4710.

(26) Kang, B.; Biswas, K. Exploring Polaronic, Excitonic Structures and Luminescence in $Cs_4PbBr_6/CsPbBr_3$. *J. Phys. Chem. Lett.* **2018**, *9*, 830−836.

(27) Roccanova, R.; Yangui, A.; Nhalil, H.; Shi, H.; Du, M.-H.; Saparov, B. Near-Unity Photoluminescence Quantum Yield in Blue-Emitting $Cs_3Cu_2Br_{5-x}I_x$ ($0 \le x \le 5$). *ACS Appl. Electron. Mater.* **2019**, *1*, 269−274.

(28) Du, M.-H. Emission Trend of Multiple Self-Trapped Excitons in Luminescent 1D Copper Halides. *ACS Energy Lett.* **2020**, *5*, 464−469.

(29) Salpeter, E. E.; Bethe, H. A. A Relativistic Equation for Bound-State Problems. *Phys. Rev.* **1951**, *84*, 1232.

(30) Wang, L.; Shi, Z.; Ma, Z.; Yang, D.; Zhang, F.; Ji, X.; Wang, M.; Chen, X.; Na, G.; Chen, S.; et al. Colloidal Synthesis of Ternary Copper Halide Nanocrystals for High-Efficiency Deep-Blue Light-Emitting Diodes with a Half-Lifetime Above 100 h. *Nano Lett.* **2020**, *20*, 3568−3576.

(31) Mott, N.; Stoneham, A. The Lifetime of Electrons, Holes and Excitons Before Self-Trapping. *J. Phys. C: Solid State Phys.* **1977**, *10*, 3391.

(32) Marian, C. M. Spin−Orbit Coupling and Intersystem Crossing in Molecules. *WIREs Comput. Mol. Sci.* **2012**, *2*, 187−203.

(33) Kohn, W.; Sham, L. J. Self-Consistent Equations Including Exchange and Correlation Effects. *Phys. Rev.* **1965**, *140*, A1133−A1138.

(34) Kresse, G.; Furthmüller, J. Efficient Iterative Schemes for *Ab Initio* Total-Energy Calculations Using a Plane-Wave Basis Set. *Phys. Rev. B: Condens. Matter Mater. Phys.* **1996**, *54*, 11169−11186.

(35) Kresse, G.; Furthmüller, J. Efficiency of *Ab-Initio* Total Energy Calculations for Metals and Semiconductors Using a Plane-Wave Basis Set. *Comput. Mater. Sci.* **1996**, *6*, 15−50.

(36) Kresse, G.; Joubert, D. From Ultrasoft Pseudopotentials to the Projector Augmented-Wave Method. *Phys. Rev. B: Condens. Matter Mater. Phys.* **1999**, *59*, 1758−1775.

https://doi.org/10.1021/acs.jpclett.1c02252
J. Phys. Chem. Lett. 2021, 12, 8447−8452

(37) Blöchl, P. E. Projector Augmented-Wave Method. *Phys. Rev. B: Condens. Matter Mater. Phys.* **1994**, *50*, 17953−17979.
(38) Marzari, N.; Vanderbilt, D. Maximally Localized Generalized Wannier Functions for Composite Energy Bands. *Phys. Rev. B: Condens. Matter Mater. Phys.* **1997**, *56*, 12847−12865.
(39) Pizzi, G.; Vitale, V.; Arita, R.; Blügel, S.; Freimuth, F.; Géranton, G.; Gibertini, M.; Gresch, D.; Johnson, C.; Koretsune, T.; et al. Wannier90 as a Community Code: New Features and Applications. *J. Phys.: Condens. Matter* **2020**, *32*, 165902.
(40) Kim, S.; Hood, S. N.; van Gerwen, P.; Whalley, L. D.; Walsh, A. Carriercapture.jl: Anharmonic Carrier Capture. *J. Open Source Softw.* **2020**, *5*, 2102.

https://doi.org/10.1021/acs.jpclett.1c02252
J. Phys. Chem. Lett. 2021, 12, 8447−8452